

Supplementary information for

**Carbene Catalysed Chirality-Controlled Site-Selective Acylation of
Saccharides**

Table of Contents

Supplementary Methods	2
1. General Information	2
2. Preparation of Catalysts	3
3. Synthesis of the Substrates	5
4. Optimization Studies	8
5. Experimental Procedures and Characterization Data	12
6. Synthetic Application	52
7. Computational Details and Mechanism Studies	59
8. Single Crystal X-Ray Diffraction	67
9. NMR spectra	69
Supplementary References	197

7. Computational Details and Mechanism Studies

7.1 Computational methods

Geometry optimizations in the gas phase were initially carried out using global hybrid functional M06-2X¹⁷ with Karlsruhe-family basis set of double- ζ valence def2-SVP^{18,19} for all atoms as implemented in *Gaussian 16* rev. A.03²⁰. Minima and transition structures on the potential energy surface (PES) were confirmed as such by harmonic frequency analysis, showing respectively zero and one imaginary frequency, at the same level of theory.

Single point (SP) corrections were performed using M06-2X functional and def2-TZVP¹⁸ basis set for all atoms. The implicit SMD continuum solvation model²¹ was used to account for the solvent effects of dichloromethane (DCM) for NHC **G**, and Diisopropylether (DIPE) for NHC *ent-G* on the overall free energy PES. Gibbs energies were evaluated at room temperature for NHC **G**, and at 0 °C for NHC *ent-G*, consistent with the experimental conditions, using a quasi-RRHO treatment of vibrational entropies^{22,23}. Vibrational entropies of frequencies below 100 cm⁻¹ were obtained according to a free rotor description, using a smooth damping function to interpolate between the two limiting descriptions. The free energies were further corrected using standard concentration of 1 mol/L, which was used in solvation calculations. SMD(DCM/DIPE)-M06-2X/def2-TZVP//M06-2X/def2-SVP Gibbs energies are given and quoted in kcal mol⁻¹ throughout. *Unless otherwise stated, these solvent-corrected values are used for discussion throughout the main text and in this supporting information.*

Non-covalent interactions (NCIs) were analyzed using NCIPLOT²⁴ calculations. The *.wfn* files for NCIPLOT were generated at M06-2X/def2-SVP^{18,19} level of theory. NCI indices calculated with NCIPLOT were visualized at a gradient isosurface value of $s = 0.5$ au. These are colored according to the sign of the second eigenvalue (λ_2) of the Laplacian of the density ($\nabla^2\rho$) over the range of -0.1 (blue = attractive) to $+0.1$ (red = repulsive). All molecular structures and molecular orbitals were visualized using *PyMOL* software²⁵.

7.2 Model reactions

For this study, we select the model reactions depicted in Figure S5 for mechanistic studies using DFT modeling.

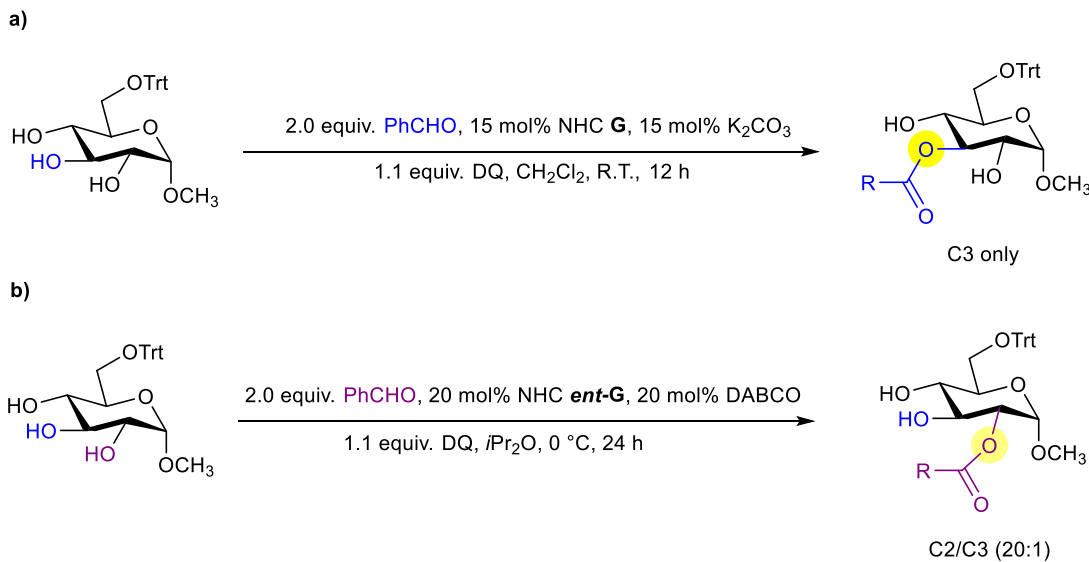


Figure S5. Model reactions used for DFT-based mechanistic studies, catalyzed by a) NHC **G**, and b) NHC **ent-G**.

7.3 Conformational considerations

Initially, we obtained the DFT optimized (M06-2X/def2-SVP level of theory) key regio-determining initial guess TSs for NHC **G** and **ent-G**, considering both (*Re*)- and (*Si*)-face attacks for each (2)-OH and (3)-OH group, resulting in a total of 8 TSs. It is important to note that these TSs were located using the base K₂CO₃ (represented as **b1**) for NHC **G** (TS_{*I*}_b1_**G**_O_{*x*}_F, where *I* = initial; *x* = 2 or 3; and *F* = *Re* or *Si*), and DABCO (denoted as **b2**) for NHC **ent-G** (TS_{*I*}_b2_**ent-G**_O_{*x*}_F), in line with the experiments. Subsequently, we utilized these DFT-optimized TS structures as input to conduct thorough conformational sampling using the *crest* program, aiming to identify the corresponding most stable TS conformers. From the sampling, we extracted the three lowest energy TS conformers (optimized at the *xtb* level) for NHC **G** and **ent-G**, resulting in a total 24 conformers. These conformers are predominantly in the chair conformation, with only one in the boat conformation, corresponding to the (*Re*)-face attack by (2)-OH for **ent-G** system. These *xtb*-optimized conformers were then reoptimized at the DFT M06-2X/def2-SVP level of theory. The most stable TS structures obtained at the DFT level are in the chair conformation. It is worth noting that we have succeeded in obtaining only 2 optimized TS structures for both the (*Re*)- and (*Si*)-face attack by (2)-OH (for NHC **G** system), and for the (*Si*)-face attack by (3)-OH (for both NHC **G** and **ent-G** systems), resulting in a total 20 stable conformers.

7.4 Mechanistic studies on the NHC **G** catalyzed model reaction

The most stable TS structures, representing both (*Re*)- and the (*Si*)-face attacks of the (2)-OH and (3)-OH groups, along with their solvent-corrected relative Gibbs energies SMD(DCM)-M06-2X/def2-TZVP//M06-

2X/def2-SVP, are presented in Figure S6 and the corresponding NCI plots are shown in Figure S7.

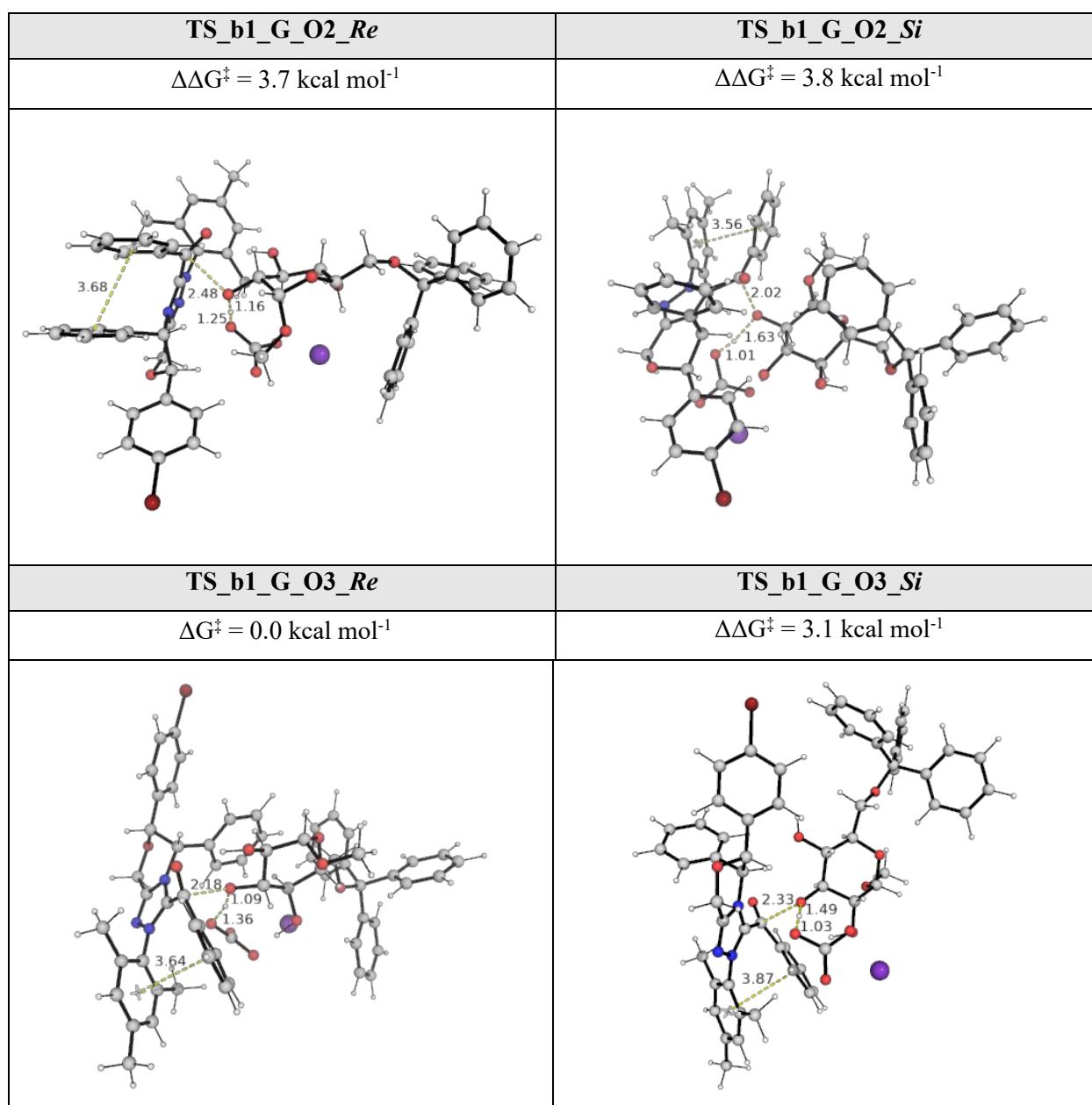


Figure S6. DFT Optimized geometries of the most stable TS structures, representing both (*Re*)- and the (*Si*)-face attacks of the 2-OH and 3-OH groups for the NHC **G** catalyzed model reaction. Key bond distances are given in Å. Relative activation barriers are given in kcal mol⁻¹ and taken relative to the lowest activation barrier.

Our DFT results indicate that the calculated TS barrier for the (3)-OH group attack at the carbonyl carbon of the acyl azolium intermediate from the (*Re*)-face, **TS_b1_G_O3_Re**, is more favorable by 3.1 kcal/mol compared to the (*Si*)-face, **TS_b1_G_O3_Si**, Figure S6. On the other hand, for the (2)-OH group, the computed TS barrier for the attack from (*Re*)-face, **TS_b1_G_O2_Re**, is lower in energy by only 0.1 kcal/mol compared (*Si*)-face, **TS_b1_G_O2_Si**. Overall, the calculated TS barriers suggest that (3)-OH

acylation via **TS_b1_G_O3_Re** has the lowest activation barrier (3.7 kcal/mol compared to (2)-OH acylation via **TS_b1_G_O2_Re**) and is therefore predicted to be kinetically most favorable, consistent with the experimentally observed C(3)-OH acylated product.

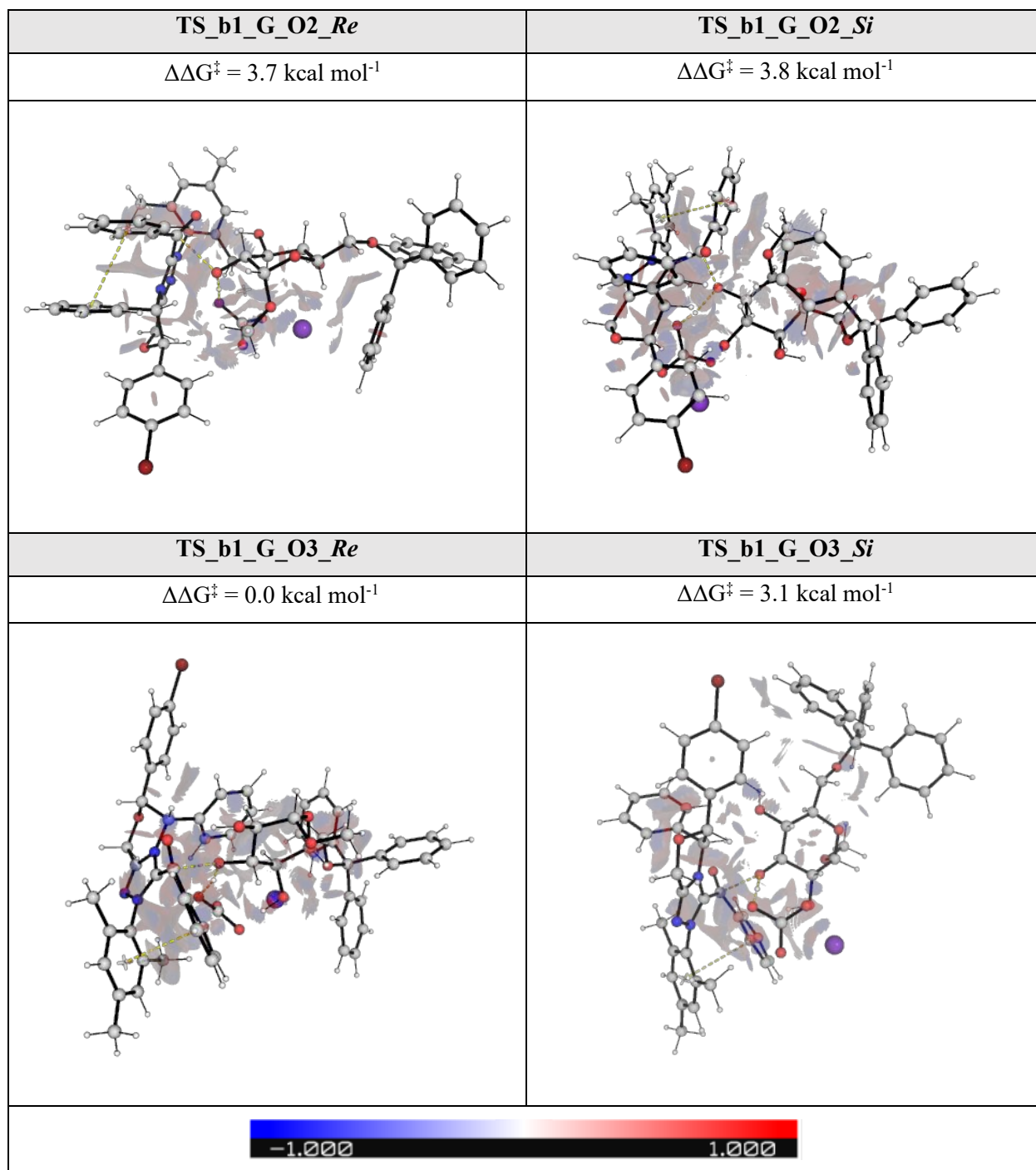


Figure S7. NCI plots of the regio-determining TSs for the NHC **G** catalyzed model reaction.

7.5 Mechanistic studies on the NHC *ent-G* catalyzed model reaction

The most stable TS structures, representing both (*Re*)- and the (*Si*)-face attacks of the 2-OH and 3-OH groups, along with their solvent-corrected relative Gibbs energies SMD(DIPE)-M06-2X/def2-TZVP//M06-

2X/def2-SVP, are presented in sFigure S8, and the corresponding NCI plots are shown in Figure S9.

For NHC *ent-G* catalyzed model reaction, the calculated TS barriers reveal that the (2)-OH group attack at the carbonyl carbon of the acyl azolium intermediate from the (*Si*)-faces, **TS_b2_ent-G_O2_Si**, is more favorable by 1.0 kcal/mol compared to the (*Re*)-face, **TS_b2_ent-G_O2_Re**, Figure S8. On the contrary, for the (3)-OH group, the computed TS barrier for the attack from the (*Re*)-face, **TS_b2_ent-G_O3_Re**, is more favorable by 0.9 kcal/mol compared to the (*Si*)-face, **TS_b2_ent-G_O3_Si**, Figure S8. Overall, these TS barriers suggest that (2)-OH acylation via the most stable **TS_b2_ent-G_O2_Si** is lower by 1.8 kcal/mol compared to (3)-OH acylation via **TS_b2_ent-G_O3_Re**, translating to an O2:O3 acylation ratio of 28:1, which agrees qualitatively well with the experimentally observed (2)-OH acylated product selectivity.

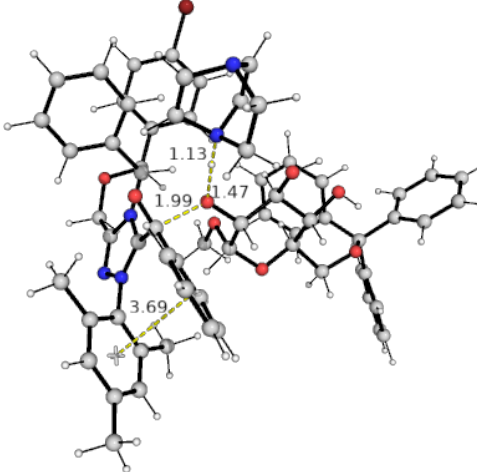
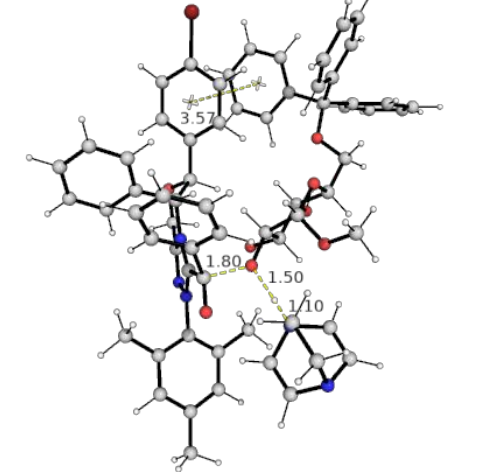
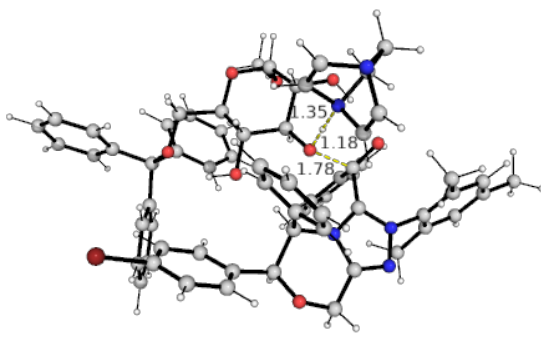
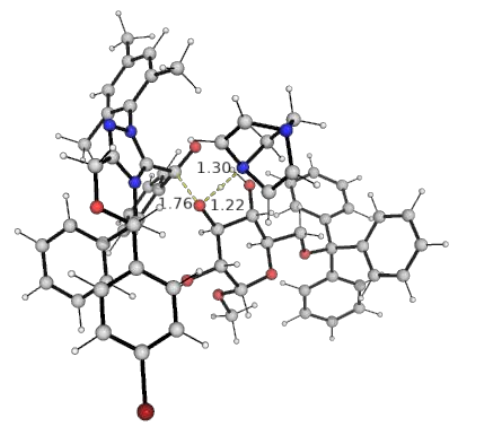
TS_b2_ent-G_O2_Re	TS_b2_ent-G_O2_Si
$\Delta\Delta G^\ddagger = 1.0 \text{ kcal mol}^{-1}$	$\Delta\Delta G^\ddagger = 0.0 \text{ kcal mol}^{-1}$
	
TS_b2_ent-G_O3_Re	TS_b2_ent-G_O3_Si
$\Delta\Delta G^\ddagger = 1.8 \text{ kcal mol}^{-1}$	$\Delta\Delta G^\ddagger = 2.7 \text{ kcal mol}^{-1}$
	

Figure S8. DFT Optimized geometries of the most stable TS structures, representing both (*Re*)- and the (*Si*)-face attacks of the 2-OH and 3-OH groups, for the NHC *ent-G* catalyzed model reaction. Key bond distances are given in Å. Relative activation barriers are given in kcal mol⁻¹ and taken relative to the lowest activation barrier.

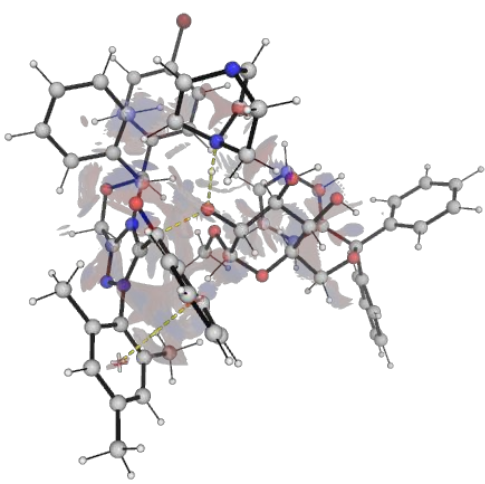
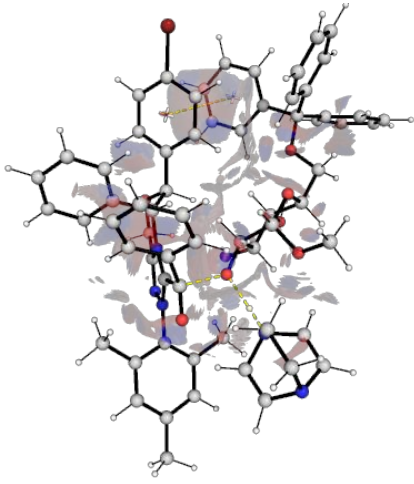
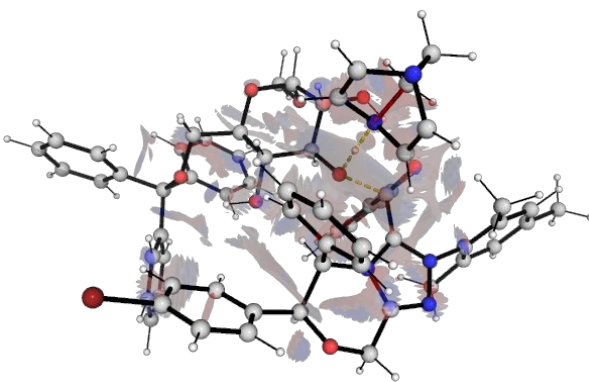
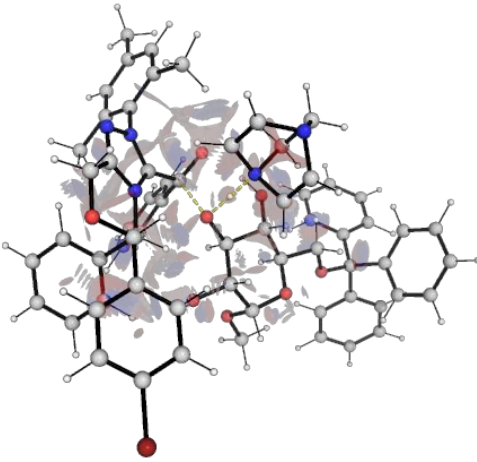
TS_b2_ent-G_O2_Re	TS_b2_ent-G_O2_Si
$\Delta\Delta G^\ddagger = 1.0 \text{ kcal mol}^{-1}$	$\Delta\Delta G^\ddagger = 0.0 \text{ kcal mol}^{-1}$
	
TS_b2_ent-G_O3_Re	TS_b2_ent-G_O3_Si
$\Delta\Delta G^\ddagger = 1.8 \text{ kcal mol}^{-1}$	$\Delta\Delta G^\ddagger = 2.7 \text{ kcal mol}^{-1}$
	

Figure S9. NCI plots of the regio-determining TSs for the NHC *ent-G* catalyzed model reaction.

7.6 Optimized structures and absolute energies, zero-point energies

Geometries of all optimized structures (in .xyz format with their associated energy in Hartrees) are included in a separate folder named *DFT_optimized structures* with an associated readme.txt file. All these data have been deposited with this Supporting Information and uploaded to <https://zenodo.org/records/13925754> (DOI: [10.5281/zenodo.13925754](https://doi.org/10.5281/zenodo.13925754)).

Absolute values (in Hartrees) for SCF energy, zero-point vibrational energy (ZPE), enthalpy and quasi-harmonic Gibbs free energy (evaluated at room temperature for NHC **G** and at 0 °C for NHC *ent-G*) for gas-phase M06-2X/def2-SVP optimized structures are given below. Single point corrections in SMD

dichloromethane for NHC **G**, and diisopropylether NHC *ent-G* using M06-2X/def2-TZVP functional are also included.

Structure	E/au	ZPE/au	H/au	T.S/au	qh-G/au	SP MN15/def2-TZVP
TS_b1_G_O2_Re_c1	-6482.470381	1.070387	-6481.33068	0.176781	-6481.48944	-6486.607811
TS_b1_G_O2_Re_c2	-6482.458832	1.071417	-6481.31899	0.172765	-6481.4748	-6486.593372
TS_b1_G_O2_Si_c1	-6482.489077	1.074799	-6481.3462	0.173198	-6481.50208	-6486.61376
TS_b1_G_O2_Si_c2	-6482.480083	1.07481	-6481.33728	0.171787	-6481.4926	-6486.606539
TS_b1_G_O3_Re_c1	-6482.481027	1.072617	-6481.34046	0.171373	-6481.49541	-6486.618437
TS_b1_G_O3_Re_c2	-6482.476233	1.071243	-6481.33601	0.176011	-6481.49394	-6486.614353
TS_b1_G_O3_Re_c3	-6482.482424	1.072185	-6481.3422	0.171353	-6481.49754	-6486.614158
TS_b1_G_O3_Si_c1	-6482.473203	1.072517	-6481.33136	0.176111	-6481.48948	-6486.611618
TS_b1_G_O3_Si_c2	-6482.492132	1.075289	-6481.3487	0.17019	-6481.50336	-6486.616287
TS_b2_ent-G_O2_Re_c1	-5961.313562	1.194141	-5960.06048	0.151676	-5960.19621	-5965.454347
TS_b2_ent-G_O2_Re_c2	-5961.315923	1.195108	-5960.06237	0.148121	-5960.19624	-5965.453577
TS_b2_ent-G_O2_Re_c3	-5961.302249	1.193763	-5960.04929	0.151318	-5960.18518	-5965.450484
TS_b2_ent-G_O2_Si_c1	-5961.318684	1.19417	-5960.06552	0.149778	-5960.20058	-5965.456698
TS_b2_ent-G_O2_Si_c2	-5961.313042	1.192271	-5960.06173	0.150514	-5960.19724	-5965.453302
TS_b2_ent-G_O2_Si_c3	-5961.305158	1.194207	-5960.05194	0.15159	-5960.18782	-5965.45246
TS_b2_ent-G_O3_Re_c1	-5961.311628	1.191416	-5960.06132	0.149342	-5960.19612	-5965.451205
TS_b2_ent-G_O3_Re_c2	-5961.31286	1.195368	-5960.05864	0.1516	-5960.19419	-5965.45194
TS_b2_ent-G_O3_Re_c3	-5961.308156	1.193886	-5960.05544	0.150496	-5960.19047	-5965.444511
TS_b2_ent-G_O3_Si_c1	-5961.298084	1.190736	-5960.04772	0.154704	-5960.18536	-5965.446983
TS_b2_ent-G_O3_Si_c2	-5961.305723	1.192962	-5960.05371	0.150705	-5960.18938	-5965.447519